MARCASITE IN BLACK SHALES—A MINERAL PROXY FOR OXYGENATED BOTTOM WATERS AND INTERMITTENT OXIDATION OF CARBONACEOUS MUDS

JUERGEN SCHIEBER

Department of Geological Sciences, Indiana University, Bloomington, Indiana 47405, U.S.A.

ABSTRACT: Black shales in the geologic record have long been considered to reflect deposition under anoxic or even euxinic conditions. Although bottom-water anoxia favors deposition of black shales, certain biological indicators, such as benthic fossils and bioturbation, suggest that bottom-water conditions may not have been as persistently anoxic as commonly presumed. Examination of twelve marine carbonaceous shale-bearing units, ranging in age from Middle Proterozoic to Cretaceous, suggests that in addition to paleontological clues, early diagenetic marcasite formed in uncompacted surficial sediments is a reliable indicator of oxygen-bearing bottom waters. Marcasite requires low pH values to form, and oxidation of already existing sedimentary pyrite provides a plausible chemical scenario to achieve that condition. In the studied examples, degraded pyrite framboids and corrosion features on pyrite grains indicate partial pyrite destruction in surface sediments, and suggest that intermittent reoxidation of earlier formed iron sulfides may indeed have generated the low pH values required for marcasite formation. Thus, observations of textures spatially associated with secondary marcasite growth are consistent with a scenario whereby oxygen in overlying sea water drove downward migration of oxidation fronts. Pervasive marcasite in black shales from a wide range of occurrences suggests multiple reoxygenation events during the deposition of these shale units and calls for more dynamic ocean circulation than previously assumed. The latter consideration may, for example, prove important for those instances where a black shale is associated with an oceanic anoxic event (OAE), because these are commonly presumed to have been deposited under fully anoxic conditions.

INTRODUCTION

Sedimentary iron sulfides have been studied in many in black shales because of linkages to redox conditions and the global biogeochemical cycles of iron, sulfur, carbon, and oxygen (Goldhaber 2003). Pyrite (FeS_2, cubic), the best known and most common iron sulfide, typically forms tiny crystallites (1 µm or less in size) that are either organized in framboids or scattered through surficial sediments. Formation of iron sulfides in pore waters requires anoxic pore waters and a supply of hydrogen sulfide from microbial sulfate reduction (Berner 1984). In addition, at low temperatures the conversion of initially formed amorphous iron monosulfides to pyrite depends on pH, and in alkaline solutions this conversion results in pyrite (Schoonen and Barnes 1991).

Marcasite (FeS_2, orthorhombic) on the other hand, the dimorph of pyrite, is rarely looked for because the comparatively high pH of surficial marine pore waters implies that pyrite formation is favored (Rickard et al. 1995; Wilkin 2003). Nonetheless, there have been occasional reports of marcasite from black shales of various ages (Siesser 1978; Cecca et al. 1994; Alvi and Winterhalter 2001; Marsaglia 2005). Marcasite has also been described from waterlogged acid sulfate soils in coastal regions (e.g., Wilson 2005; Bush et al. 2004; Luther and Church 1988). In the latter examples, low pH values were attributed to either the presence of organic acids (Bush et al. 2004) or to oxidation of pyrite (Luther and Church 1988). Given that experimental work by Schoonen and Barnes (1991) has shown that in low-temperature acidic solutions both pyrite and marcasite form, and that below pH 5 marcasite dominates because of its higher growth rate, there likely are mechanisms that can produce low-pH pore waters in marine sediments.

Recent studies of marine lag deposits show marcasite as overgrowths on reworked and corroded pyrite debris, such as concretions and pyritic burrow tubes (Schieber and Riciputi 2005; Schieber 2007). Based on petrographic features and chemical considerations, these studies suggest that oxidation and dissolution of reworked pyrite grains raised concentrations of dissolved iron and lowered pH sufficiently to enable marcasite formation (Murowchick and Barnes 1987: Schoonen and Barnes 1991; Benning et al. 2000) in surficial pyritic lags.

In this paper, the textures of marcasite in marine black shales of Proterozoic to Cretaceous age are interpreted to indicate that this marcasite formed in uncompacted water-rich mud as an early diagenetic precipitate. Many of these black shales were once thought to have been deposited under fully anoxic conditions. Based on marcasite textures and earlier work on marcasite in marine lag deposits (Schieber and Riciputi 2005; Schieber 2007), a case is being made that these shales may actually have experienced intermittent reoxidation early in their depositional history.

MATERIALS AND METHODS

Samples of marine black shale ranging in age from Middle Proterozoic to Cretaceous (Table 1) were examined for marcasite. Samples were polished to 0.1 µm on diamond-coated polishing film and examined by reflected-light microscopy with a high-power (100 ×) oil-immersion objective. Iron sulfide grains that showed optical properties characteristic of marcasite, such as pleochroism (plane-polarized light) and anisotropy (crossed polarizers) were then examined under an electron microscope

TABLE 1.— *Marcasite Occurrences in Various Shale Units.*

Unit & Age	Location	Lithology	Features	Timing
Bonarelli Horizon Cretaceous, Cenomanian	Umbria, Italy	black shale	degraded pyrite framboids euhedral μm-size marcasite	Early, water-rich muds, via differential compaction
Eagleford Shale Cretaceous, Cenomanian	Texas, USA	black shale	degraded pyrite framboids euhedral μm-size marcasite tabular-bladed marcasite	Early, water-rich muds, via differential compaction
Selli Interval Cretaceous, Aptian	Shatsky Rise, Pacific ODP Leg 198, Site 1207 (Dumitrescu and Brassell 2005; Dumitrescu 2006)	black shale	degraded pyrite framboids euhedral μm-size marcasite	Early, water-rich muds, via differential compaction
Posidonia Shale Jurassic, Toarcian	SW Germany	black shale	degraded pyrite framboids euhedral μm-size marcasite	Early, water-rich muds , via differential compaction
Jet Rock Jurassic/Toarcian	England	black shale	degraded pyrite framboids euhedral μm-size marcasite	Early, water-rich muds, via differential compaction
Cisco Formation Pennsylvanian	Texas (Sur 2009)	black shale	Radial-bladed marcasite overgrowing spherical pyrite grains	Early, water-rich muds
Barnett Shale Mississippian	Texas, USA (Milliken et al. 2007)	black shale	degraded pyrite framboids euhedral μm-size marcasite tabular-bladed marcasite	Early?, in winnowed lags with marcasite
Cleveland Shale Devonian, Famennian	Kentucky, USA (Schieber and Lazar, 2004)	black shale	degraded pyrite framboids euhedral μm-size marcasite tabular-bladed marcasite	Early, water-rich muds, via differential compaction
New Albany Shale Devonian, Frasnian	Indiana, USA (Schieber and Lazar 2004)	black shale	degraded pyrite framboids euhedral μm-size marcasite tabular-bladed marcasite	Early, water-rich muds, via differential compaction, in winnowed lags with marcasite
Winnipeg Formation Lower Ordovician	Saskatchewan, Canada (Schieber and Riciputi 2005)	gray shale	degraded pyrite framboids euhedral micron-size marcasite	Early, water-rich muds, in primary pyrite-marcasite ooids
Powers Steps Formation Lower Ordovician	Newfoundland, Canada (Ranger et al. 1984)	black shale	degraded pyrite framboids euhedral μm-size marcasite	Early?, water-rich muds, in winnowed lags with marcasite
Bijaygar Shale Late Proterozoic (1.1 Ga; Ray 2006)	Northern India, Vindhyan Supergroup (Schieber et al. 2007)	black shale	euhedral μm-size marcasite	Early, water-rich muds, via differential compaction

Examples of black-shale-bearing stratigraphic units discussed and illustrated in the manuscript.

(FEI Quanta FEG 400) with an electron backscatter diffraction detector (EBSD, HKL Nordlys system). EBSD was used to confirm the presence of marcasite and to map the distribution of pyrite and marcasite within iron sulfide grains (Schieber 2007a) as small as a few micrometers in diameter. For a single analysis, the analyzed area depends on the beam diameter and the sample tilt. The Nordlys system operates at a 70° sample tilt, and in this geometry a beam of 1 nm diameter would result in a 1 nm × 3 nm area to be analyzed. At smaller beam diameters the analyzed area is correspondingly smaller. In the SEM that was used for this study, the beam diameter is variable and below 1 nm in high-resolution setting and can generate EBSD diffraction (Kikuchi) patterns from nanometer-size regions of the sample.

OBSERVATIONS

Black shales from eleven stratigraphic units, eight geologic time intervals (Cenomanian to Middle Proterozoic), three continents, and one modern ocean basin were examined for marcasite (Table 1). Although only a subset of these is described in some detail here, marcasite occurs in all units (Table 1). Whereas in some samples marcasite had undergone partial pyrite inversion, in the majority of samples marcasite domains were large enough to be identified with an optical microscope.

Devonian Black Shales of the Eastern U.S.

The most extensively studied sample set, Devonian black shales of the eastern USA, includes multiple locations and the entire stratigraphic range of these black shales (Table 2; Fig. 1). Observations were made on a collection of more than 1,000 polished thin sections, many of which contain agglutinated benthic foraminifera and attest to bottom waters

that were likely oxygen depleted but not wholly anoxic (Schieber 2009). The underlying rationale for the use of this sample set is that it links the observed marcasite to samples that are likely to record intermittent reoxidation of surficial sediments and thus are an ideal natural laboratory to assess sedimentary marcasite formation.

This data set (Schieber 2009) includes three locations where the entire Frasnian to Famennian black shale interval was examined via closely spaced thin sections (Fig. 1) and contains representatives of most of the regionally significant Devonian black shale intervals in the eastern USA. At the reference section of the Chattanooga Shale (Conant and Swanson 1969) in DeKalb County, Tennessee, 56 thin sections were spaced over 9.5 meters of a highly condensed section, and all the thin sections of black shales contained variable amounts of disseminated marcasite. In drill cores from Daviess County, Indiana, and Saline County, Illinois (Fig. 1), 48 and 49 thin sections were spaced over 39 and 49 meters of section respectively. In both locations, thin sections from all black shale intervals contained evidence of disseminated marcasite and marcasite concretions of variable size (millimeters to centimeters). Some stratigraphic intervals in these densely sampled sections are missing due to intermittent local erosion in the Devonian (Schieber and Lazar 2004). For these missing intervals, adjacent exposures and drill cores supplied sample material for examination. The sample coverage was less dense for other localities (Fig. 1), but thin sections were available for the black shale portions of each stratigraphic unit.

Marcasite was detected in every black shale sample and is closely associated with irregular patches of pyrite microcrysts and remnant spherical shapes consisting of pyrite microcrysts (Fig. 2A). Features such as remnant spherical shapes (Fig. 2A) and surface corrosion associated with framboid surfaces (observed, but not pictured for Devonian examples; see below for a Cretaceous example) suggest degradation of

TABLE 2.— *Devonian sample localities.*

#	Location	Unit	Age	Type
1	South Crosby, Yates Cty., NY	Sonyea Group	lower Frasnian	outcrop
2	Tener Mountain, Adams Cty., OH	Ohio Shale & Cleveland Shale	Famennian	outcrop
3	KEP-3, Adams Cty., KY	Ohio Shale & Cleveland Shale	Famennian	KGS drill core
4	Morehead, Rowan Cty., KY	Ohio Shale & Cleveland Shale	Famennian	outcrop
5	Irvine, Estill Cty., KY	Ohio Shale & Cleveland Shale	Famennian	outcrop
6	Burkesville, Cumberland Cty., KY	Chattanooga Shale, Gassaway Member	Famennian	outcrop
7	Core 763, Bartholomew Cty., IN	New Albany Shale	Frasnian & Famennian	IGS drill core
8	Humphrey #1, Lawrence Cty., IN	New Albany Shale	Frasnian & Famennian	UPR drill core
9	Wiseman #1, Harrison Cty., IN	New Albany Shale	Frasnian & Famennian	UPR drill core
10	Core 873, Daviess Cty., IN	New Albany Shale	Frasnian & Famennian	IGS drill core
11	Core 26376, Saline Cty., IL	New Albany Shale	Frasnian & Famennian	ILGS drill core
12	Eidson, Hawkins Cty., TN	Chattanooga Shale	Frasnian & Famennian	outcrop
13	Rock Haven, Grainger Cty., TN	Brallier Formation	Frasnian & Famennian	outcrop
14	Thorn Hill, Grainger Cty., TN	Chattanooga Shale	Frasnian & Famennian	outcrop
15	Celina, Clay Cty., TN	Chattanooga Shale, Gassaway Member	Famennian	outcrop
16	Westmoreland, Sumner Cty., TN	Chattanooga Shale	Frasnian & Famennian	outcrop
17	Chestnut Mound, Smith Cty., TN	Chattanooga Shale	Frasnian & Famennian	outcrop
18	Hurricane Bridge, DeKalb Cty., TN	Chattanooga Shale	Frasnian & Famennian	outcrop
19	Woodbury, Cannon Cty., TN	Chattanooga Shale	Frasnian & Famennian	outcrop
20	Noah, Coffee Cty., TN	Chattanooga Shale	Frasnian & Famennian	outcrop
21	Pegram, Cheatham Cty., TN	Chattanooga Shale	Frasnian & Famennian	outcrop
22	Olive Hill, Hardin Cty., TN	Chattanooga Shale	Frasnian & Famennian	outcrop
23	Lancaster, Erie Cty., NY	Oatka Creek Shale	Givetian	outcrop

KGS = Kentucky Geological Survey; IGS = Indiana Geological Survey; ILGS = Illinois Geological Survey; UPR = Union Pacific Resources; NY = New York; OH = Ohio; KY = Kentucky, IL = Illinois; IN = Indiana; TN = Tennessee

pyrite framboids. Marcasite forms either clusters of equant euhedral grains (Fig. 3A) or aggregates of tabular crystals (Fig. 2A, B, C). These morphologies, as well as spearhead twinning and well developed cleavage (Fig. 3B), help to differentiate marcasite from pyrite under the petrographic microscope and the SEM (Ramdohr 1980; Bush et al. 2004). Other diagenetic minerals intimately associated with marcasite formation are kaolinite (Fig. 2B) and quartz (Fig. 3B). Differential compaction around clusters of marcasite grains (Figs. 2A, C, 4B) is a common observation in the Devonian sample set as well as in the other examples.

Water Content and Differential Compaction.—The degree of differential compaction can be used to derive sediment water contents at the time of marcasite formation, and as such is critical for determining the timing of marcasite formation in burial history. Because it greatly helps the understanding of the described shale textures, the underlying methodol-
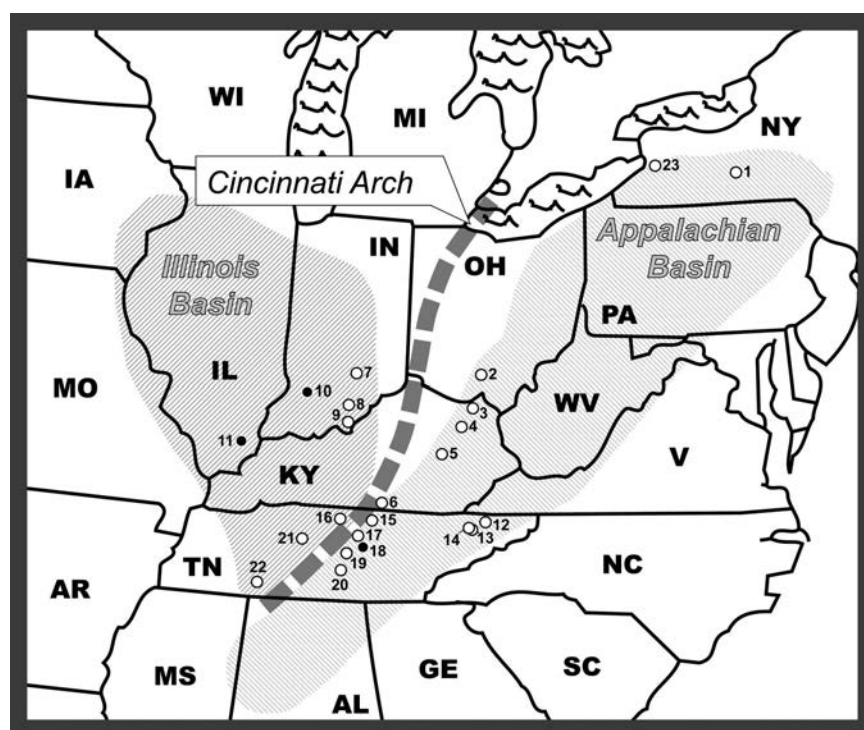

FIG. 1.—Overview map of sampling locations for Upper Devonian black shales in the eastern United States, marked by their outlines and the postal state identifier. The numbers next to sample localities (circles) refer to the location list (Table 1). Full circles (black with white rim) indicate localities where closely spaced samples were examined over the entire Frasnian–Famennian interval. The Illinois and Appalachian Basins are outlined with shading. The dashed line marks the Cincinnati Arch, a positive element that was intermittently flooded during the Late Devonian.
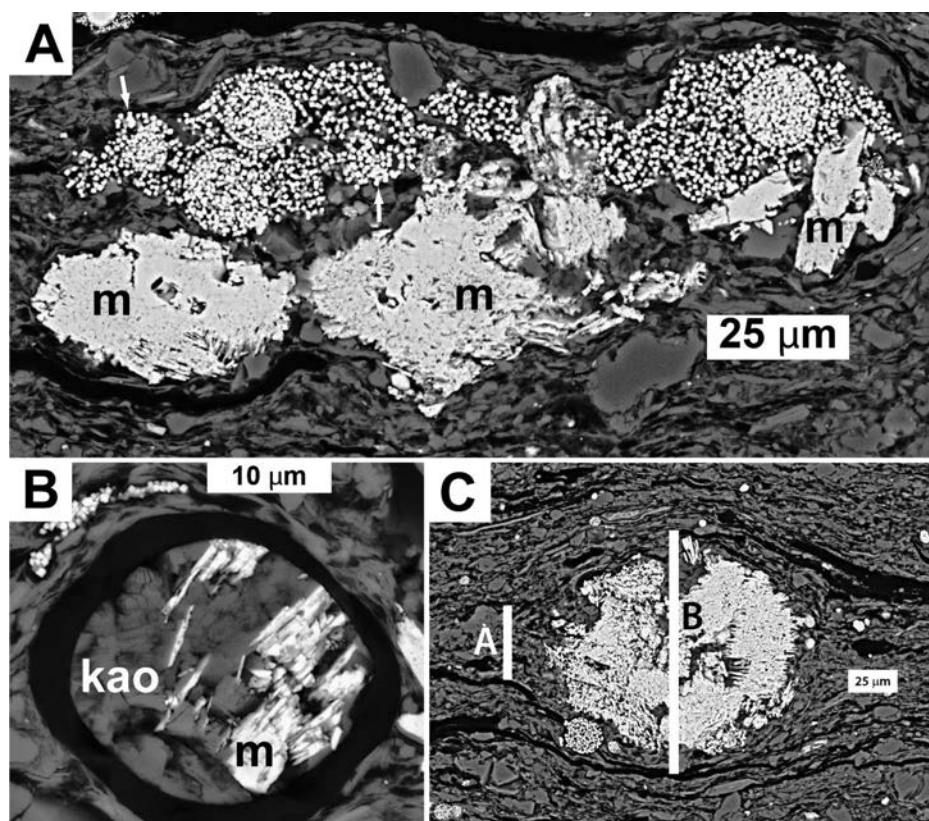
Fig. 2.—Marcasite in Upper Devonian black shales. **A)** Cleveland Shale (Kentucky)— coarse marcasite with tabular-bladed morphology ("m") shows differential compaction around marcasite clusters. Remnant spherical shapes (arrows) are interpreted as degraded (partially dissolved) pyrite framboids. **B)** Organic cyst, filled with marcasite (m) and kaolinite. Cysts are hollow and soft at the time of deposition. Spherical shape suggests mineral infill very early in diagenesis (prior to compaction) in water-rich soupy muds (Schieber and Baird 2001), because otherwise compaction would have flattened the soft and deformable cyst. **C)** Differential compaction around a marcasite cluster. Tracing laminae around the cluster (see text) reveals an initial water content of 70 vol.% from the length ratio of vertical bars A and B.

ogy is explained here using the Devonian examples. The same approach was also used in the other examples (Table 1).

Differential compaction around clusters of marcasite grains (Figs. 2A, C, 4B) is analogous to differential compaction around concretions in mudstone successions (e.g., Füchtbauer 1988). Comparison of the vertical spacing of laminae directly next to a marcasite cluster with the spacing of these laminae in the center portion of the cluster provides a means to evaluate the original water content of the sediment at the time when the marcasite cluster formed. In the case of the examined Devonian black shales, differential compaction (Fig. 2C) suggests water contents of approximately 65–75 vol %.

Similarly, organic algal cysts and spore casings are typically of rounded outline and hollow when freshly deposited. Yet, because of their soft and easily deformed consistency, they are readily flattened once compaction commences. Marcasite infills of algal cysts (Fig. 2B) and spores therefore indicate formation in uncompacted watery sediments. Petrographic study of iron-sulfide-filled algal cysts in a previous study of Devonian black shales led Schieber and Baird (2001) to conclude that the cysts were filled
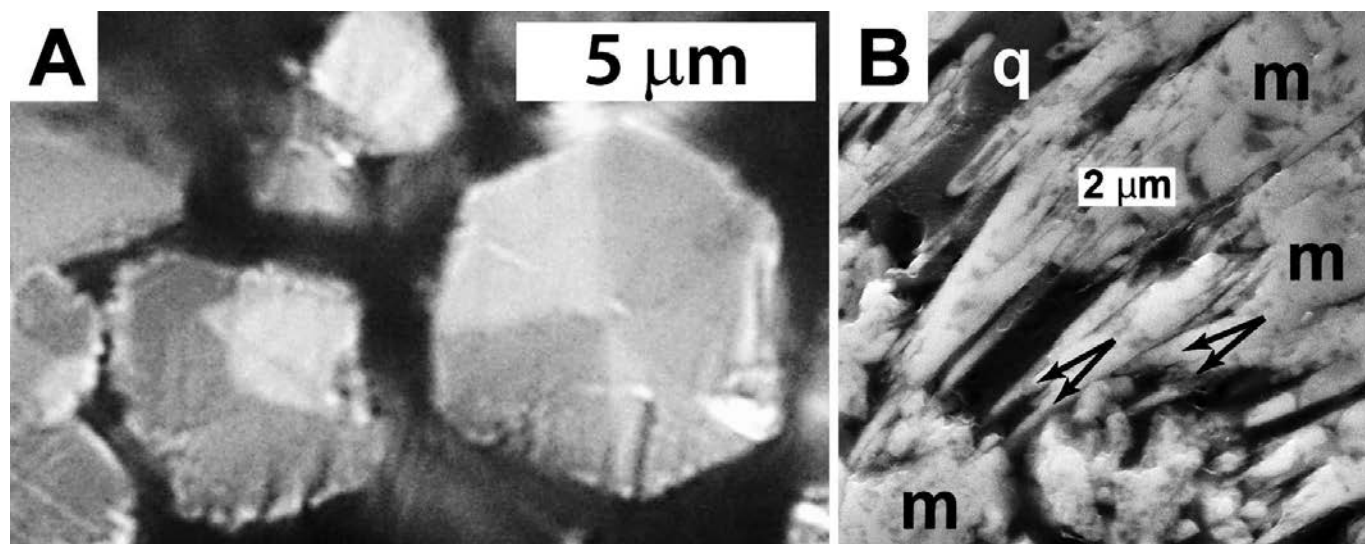

Fig. 3.—Marcasite in Upper Devonian black shales. **A)** Marcasite grains in the New Albany Shale of Indiana show anisotropy and sector zoning (crossed polarizers). **B)** Quartz cement ("q") and spearhead twinning (double arrows) of marcasite.
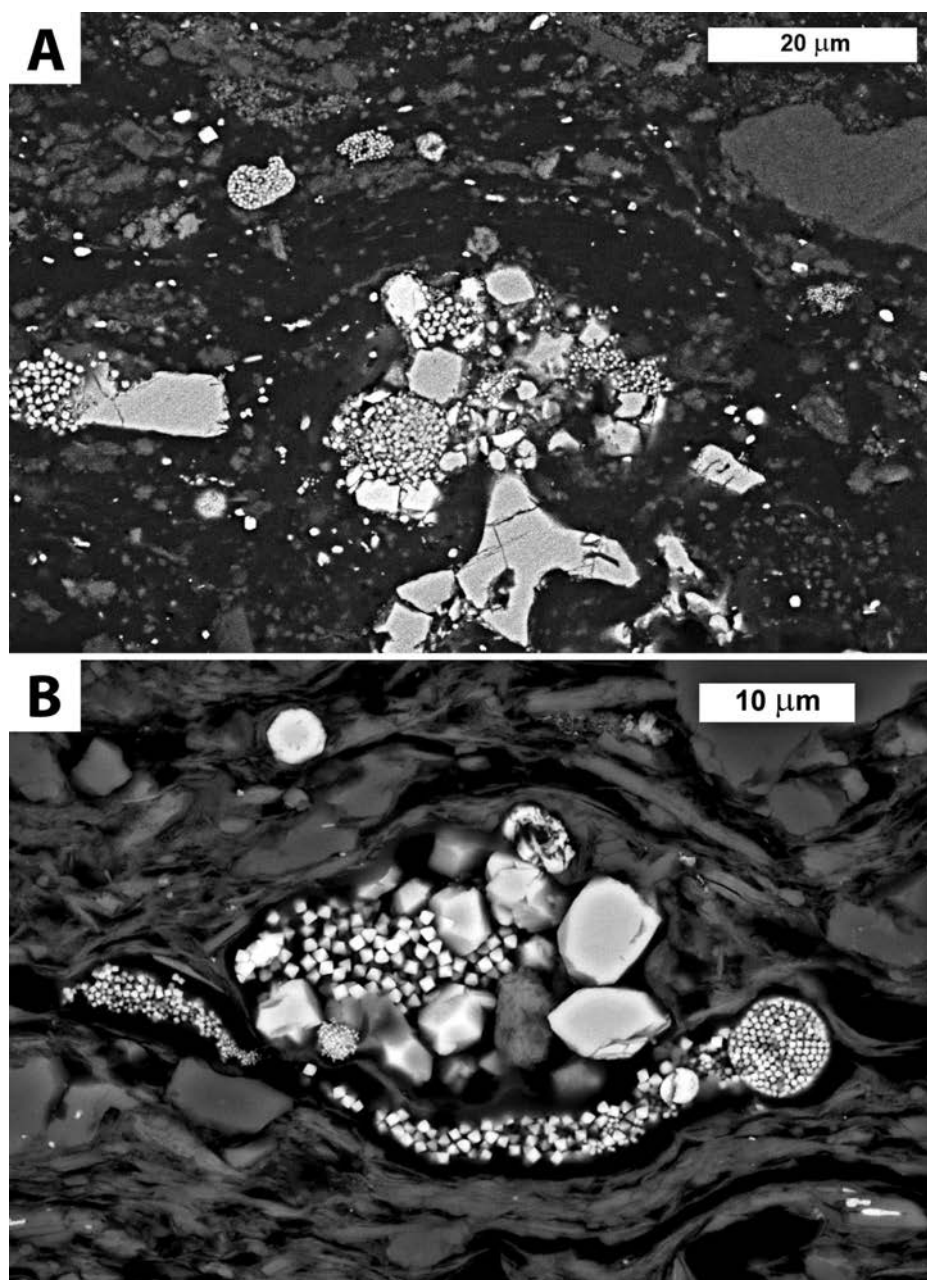
Fig. 4.—Differential compaction around pyrite-marcasite clusters. **A)** From the top portion of the Selli interval (OAE2) black shale from ODP Site 1207. **B)** From the Cleveland Shale in Kentucky. Note in both images the close spatial association among euhedral marcasite grains, patches of pyrite grains, framboids, and remnant spherical shapes (interpreted as degraded pyrite framboids). As discussed in the text, decompaction estimates suggest water contents of approximately 70 vol.% at the time of marcasite formation.

when the surrounding sediment contained 65–75 vol% water. Studies of the compaction of bioturbation features in Devonian shales of the eastern US indicate that the uppermost 10–20 centimeters of the sediment column included water contents in that range (Lobza and Schieber 1999). Thus, it appears that marcasite in the studied Devonian examples formed in surficial muds (uppermost 10–20 cm) that contained approximately 70 vol% water and constituted what has been aptly described as "soup-ground" (Goldring 1995).

Importance of Persistent Marcasite.—In these Devonian shales, marcasite is persistent throughout the entire thickness of uninterrupted black shale intervals that measure multiple meters in thickness. This observation suggests that marcasite-forming conditions must have occurred frequently enough so that every portion of a gradually subsiding multi-meter black shale interval was affected at least once. This line of reasoning also applies to the other examples presented here (Table 1).

Cretaceous Black Shales

Sedimentary marcasite is also evident in Cretaceous black shales of OAE1 and OAE2 (Hallam and Wignall 1997), from Texas, Italy, and ODP Site 1207 (Table 1). Although some of the original marcasite grains in these samples have inverted to pyrite, many of them still show the pleochroism and anisotropy (Fig. 5A) that petrographically identifies them as marcasite (Ramdohr 1980). Marcasite in OAE1 (Selli interval; ODP Site 1207) was first reported by Marsaglia (2005), measured shipboard by XRD (Fig. 6). Marcasite was also detected in organic extraction residues (seven samples provided courtesy of Mirela Dumitrescu, Fig. 6) that remained from biomarker research by Dumitrescu and Brassell (2006). To understand the petrographic context of this marcasite, eight additional samples were collected from ODP core 1207B-44R, thin sectioned, and polished, and examined by SEM. EBSD examination of thin sections and powders shows that pyrite and marcasite occur in all
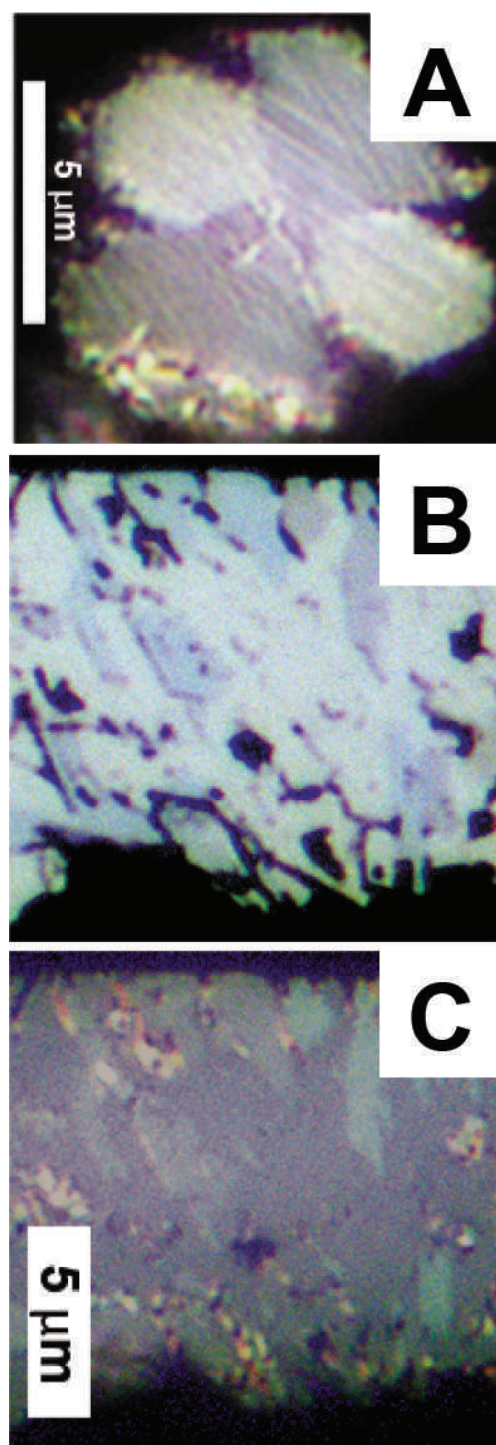
FIG. 5.—Marcasite in the Selli interval (OAE1) at ODP Site 1207 (Shatsky Rise), core 44R. **A)** Reflected-light microscopy with crossed polarizers shows anisotropy in cluster of marcasite crystals. B, C, marcasite-replaced fishbone fragment. **B)** Plane-polarized light, illustrating pleochroism of interlocking marcasite crystals. **C)** Same spot with crossed polarizers, illustrating anisotropy of marcasite grains.
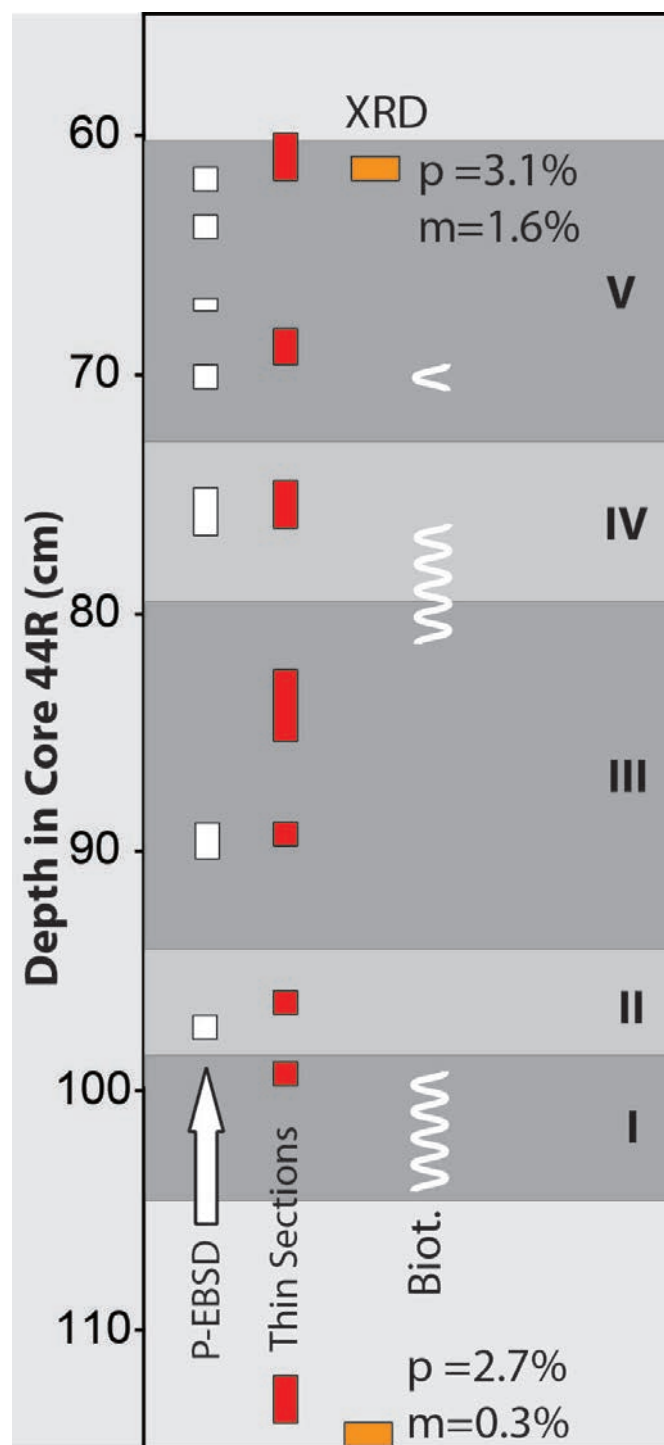

FIG. 6.—Marcasite in the Selli interval (OAE1) at ODP Site 1207 (Shatsky Rise), core 44R. Summary graphic of the subsections of this interval (I through V) as discussed by Dumitrescu et al. (2006), including marcasite and bioturbation. Wavy lines = macroscopic bioturbation (Biot.), suggestive of times when bottom waters were sufficiently oxygenated to allow macrobenthos to colonize the seafloor. White rectangles = marcasite in mineral powders from organic extractions (EBSD), red rectangles = marcasite in polished thin sections (EBSD and optical), orange rectangles = stratigraphic position of marcasite-bearing samples reported by Marsaglia (2005); p and m indicate pyrite and marcasite percentages in these latter samples.
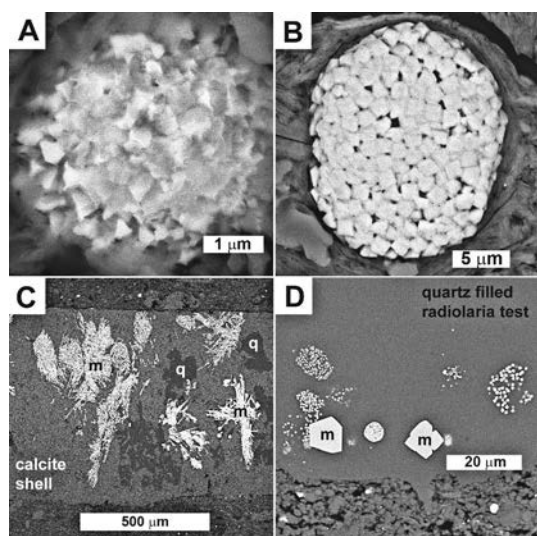
examined samples (Fig. 6). In all Cretaceous examples (Table 1) marcasite is seen to replace calcitic (Fig. 7C) and phosphatic fossil (Fig. 5B, C) debris, suggesting that marcasite precipitation occurred in tandem with dissolution of calcite and phosphate. In addition, marcasite

FIG. 7.—**A)** Surface corrosion in pyrite framboid from Cenomanian Eagleford Shale, West Texas. **B)** Smooth surface of a noncorroded framboid for comparison. It shows the tight packing of pyrite crystallites that is typical for pyrite framboids. **C)** Calcite shell in Eagleford Shale that has been partially replaced by marcasite (bright blades and needles, "m") and quartz (dark gray, "q"). **D)** Quartz-filled radiolarian test from the Bonarelli horizon (Cenomanian of Italy) with remnant spherical shapes (arrows) that are interpreted as degraded (partially dissolved) pyrite framboids.

precipitates show intimate spatial association with early diagenetic fine crystalline quartz (Figs. 7C, 8B).

The Cretaceous black shales show features that suggest degradation of pyrite framboids, such as remnant spherical shapes (Figs. 8A, 7D) and surface corrosion associated with framboid surfaces (Fig. 7A). Marcasite forms clusters of equant grains (Fig. 8A) as well as clusters of tabular and needle-like crystals (Figs. 8B, 7C). Analysis of differential compaction of shale around clusters of marcasite grains (Fig. 4A; see above) suggests early diagenetic marcasite growth at water contents comparable to the Devonian examples (Fig. 2C), most likely in surficial mud.

Proterozoic Black Shales

In this study, the oldest evidence for early diagenetic marcasite occurs in the unmetamorphosed 1.1 Ga Bijaygarh Shale of India. This shale contains abundant early diagenetic fine crystalline pyrite that follows laminae (Schieber et al. 2007), as well as early diagenetic pyrite-marcasite micro-concretions with internal corrosion features that are overgrown by secondary marcasite (Fig. 9B, C). Differential compaction around these concretions (Fig. 9A) indicates that these pyrite-marcasite concretions formed when the sediment still contained approximately 70 vol. % water.

Other Examples

Beyond these extensively studied examples, spot checks for marcasite were also conducted on thin-section collections from other shale units, including the Toarcian Posidonia Shale of southwest Germany, the Toarcian Jet Rock Formation of England, the Pennsylvanian Cisco Formation of Texas, the Mississippian Barnett Shale of Texas, thin shale intervals in the Ordovician Winnipeg Formation of Saskatchewan, and carbonaceous shales in the Ordovician Power Steps Formation of Newfoundland (Table 1).

The carbonaceous shales from this sample set showed the presence of marcasite as well, and also display the same assemblage of textural features. For example, thin sections from the Posidonia Shale show collapsed framboids, remnant spherical shapes of sub-micrometer pyrite grains, and equant, euhedral marcasite grains (Fig. 10). Samples of a carbonaceous shale from the Cisco Formation (Sur 2009) show well developed radial overgrowth of marcasite blades that cover a central pyritic body, possibly a cemented pyrite framboid (Fig. 11A). SEM examination of the Barnett Shale shows clusters of tabular marcasite that resemble those seen in the Cleveland Shale (Fig. 2), as well as a close spatial association of carbonate dissolution and silica precipitation with marcasite (Fig. 11B). Carbonaceous shales of the Powers Steps Formation of Newfoundland show remnant spherical shapes that are interpreted as degraded pyrite framboids, pyrite patches, marcasite as euhedral equant grains or as overgrowth on pyrite framboids, differential compaction around marcasite-bearing regions, and a close spatial association between marcasite and early diagenetic quartz (Fig. 12).

DISCUSSION

A survey of Eh and pH conditions in modern sediments, as well as the occurrence of marcasite in coal deposits and weathering sulfide ores, led Krumbein and Garrels (1952) to the conclusion that acidic bog or peat-producing environments were settings conducive to diagenetic marcasite formation in sediments. This view of marcasite formation in sediments is bolstered by soil-science research that associates marcasite formation with waterlogged acid sulfate soils in coastal settings (Luther and Church 1988; Bush et al. 2004; Wilson 2005). A search of the soil-science literature, however, did not yield a specific declaration of a causal link between pyrite oxidation and marcasite formation. In marine settings, alkaline seawater is generally thought to preclude early diagenetic marcasite formation (e.g., Rickard et al. 1995). Though marcasite has been identified repeatedly in marine sediments (Siesser 1978; Cecca et al. 1994; Alvi and Winterhalter 2001; Marsaglia 2005), its broader significance was left unexplored.

Research on oil-field brines and pore-water evolution during burial of sedimentary successions (e.g., Hayes 1991; Surdam et al. 1989; Surdam et al. 1991) suggests that during burial diagenesis, decarboxylation of kerogen produces carboxylic and phenolic acids in the temperature range from $80°$ to $120°$ C (MacGowan and Surdam 1990). This process leads to secondary porosity due to the destruction of carbonates (e.g., Hayes 1991; Surdam et al. 1991). From the perspective of the low-pH conditions that favor marcasite precipitation (Murowchick and Barnes 1987), a burial-diagenesis scenario can certainly lead to marcasite formation in sediments. In the examples presented here, however, that mechanism can be excluded because textural features like differential compaction around marcasite clusters and algal cysts that were infilled prior to compaction (Figs. 2B, C, 4, 9A) indicate that marcasite precipitated in water-rich surficial sediments.

Under the microscope, the samples show neither textural nor mineralogical signs of metamorphism. Iron-sulfide-mineral morphologies suggestive of marcasite were observed in samples of slate, but subsequent EBSD analysis showed that no marcasite remained. It appears thus that in the absence of metamorphism, marcasite can persist in sedimentary rocks for time periods in excess of one billion years. Ramdohr (1980) suggested this result previously on the basis of heating experiments.

Pyrite and marcasite formation requires reducing pore waters, H_2S production, and a source of iron. Beyond these conditions, experimental studies suggest that marcasite also requires low pH ($\sim$ 4 to 5) (Schoonen and Barnes 1991; Murowchick and Barnes 1987; Benning et al. 2000). A literature survey of pH in surficial marine muds indicates an absence of pH values below 6.4, and also suggests that chemical reactions associated with microbial organic-matter decay are not likely to produce the needed pH drop. Typical anoxic marine sediments are buffered in the range of pH 7 to 8 by the byproducts of organic decomposition, sulfate reduction,
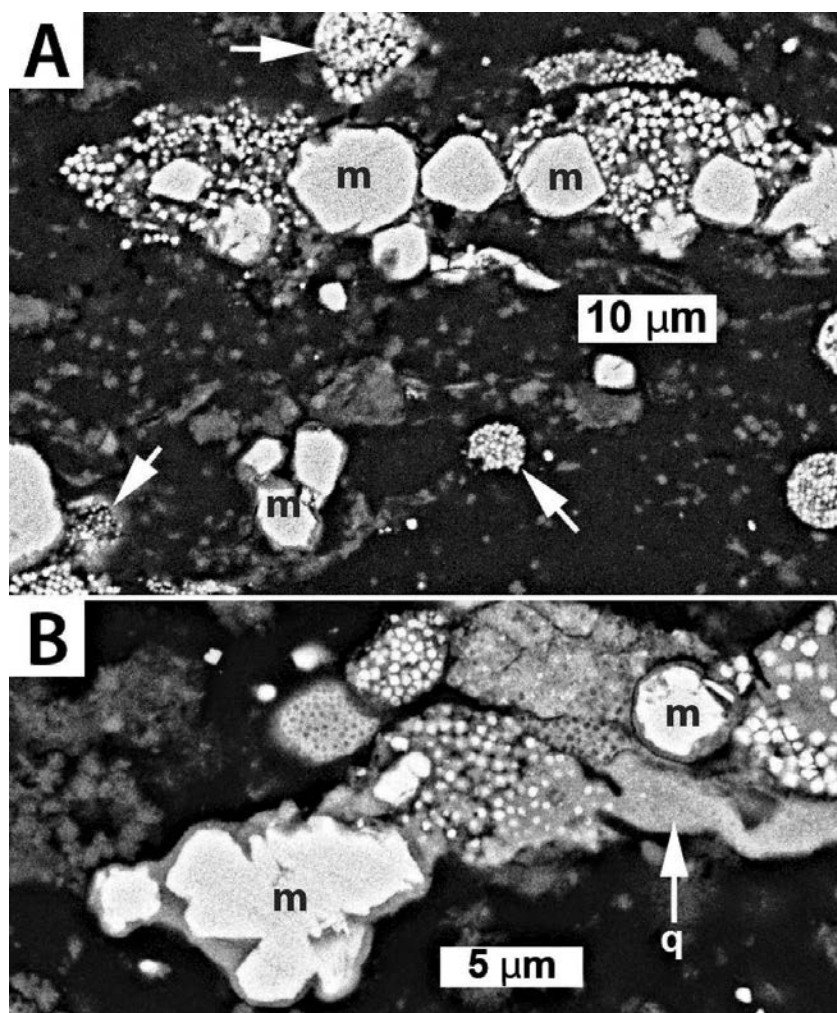
FIG. 8.—Marcasite in the Selli interval (OAE1) at ODP Site 1207 (Shatsky Rise), core 44R. **A)** A streak of fine-crystalline pyrite and marcasite in upper half of image. Marcasite grains marked m (verified with EBSD). Arrows point to remnant spherical shapes that are interpreted as degraded framboids (BSE image). **B)** Intimate spatial association between early diagenetic quartz (light gray, arrow), pyrite framboids and patches, and marcasite (m).

iron reduction, and sulfide and carbonate precipitation (Ben-Yaakov 1973; Coleman 1985).

The alkalinity of seawater precludes the direct authigenic formation of marcasite, and pyrite is the first stable iron sulfide that forms in anoxic sediments. Thus, in surficial mud, the most plausible way to simultaneously provide dissolved iron and produce the low-pH conditions needed for marcasite formation is the oxidation of previously formed sedimentary pyrite by the reaction
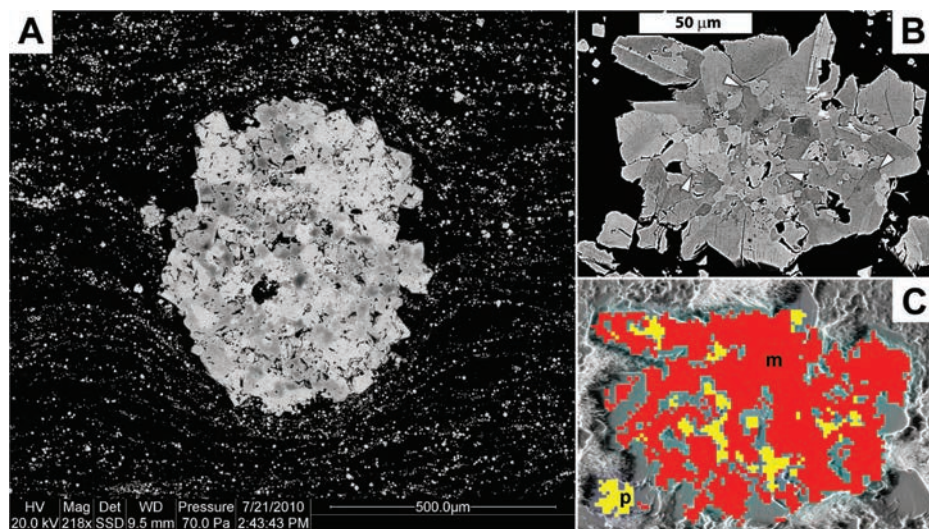

FIG. 9.—Microconcretions of pyrite and marcasite in the mid-Proterozoic Bijaygarh Shale of India. **A)** SEM photomicrograph of differential compaction around a pyrite-marcasite concretion. Image taken in backscatter electron (BSE) mode at high-contrast setting. Concentrations of iron sulfide grains (pyrite and marcasite) mark fine laminae. Differential compaction marked by these laminae suggests a water content of 70 vol.% prior to compaction. **B)** Another micro-concretion along a lamina plane with a radial cluster of iron sulfide crystals. Gray shades are an indication of orientation difference, notable at high-contrast BSE settings. White arrows point to irregular contacts that are interpreted as corrosion surfaces when prior sulfides were destroyed by oxidation. **C)** Same grain photographed at 70 degree tilt (for EBSD observations) and with an overlay of an EBSD map. Red is marcasite (m), yellow is pyrite (p). Most of this iron sulfide-cluster still consists of marcasite.
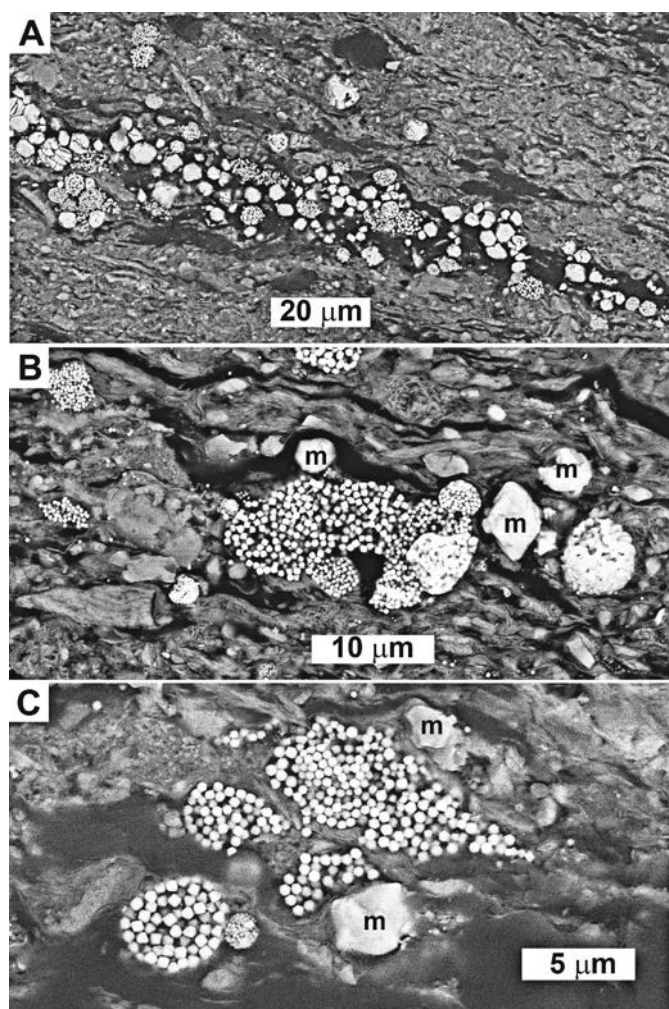
FIG. 10.—SEM backscatter images of marcasite in the Toarcian Posidonia Shale of southwest Germany. **A)** Overview of a streak of pyrite framboids, pyrite patches, remnant spherical shapes, and marcasite (the equant, euhedral crystals). **B)** Close-up of collapsed framboids and marcasite ("m"). **C)** Another close-up of collapsed framboids, remnant spherical shapes, pyrite patches, and marcasite ("m"). Marcasite was identified with EBSD.

$$FeS_2 + 3.5O_2 + H_2O \quad Fe^{2+} = 2SO_4^{2-} + 2H^+ \tag{1}$$
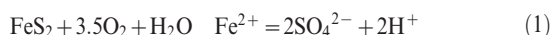
Such a scenario for decreasing pH is consistent with observations of carbonate dissolution due to iron-sulfide oxidation in modern muds (Reaves 1986) and the recognition of alternating corrosion and marcasite growth in iron sulfides from marine lags (Schieber and Riciputi 2005; Schieber 2007).

Oxidation of H_2S, for example at the redox interface and near localized sites of H_2S production, can also produce acidity. In balance, however, it is probably not important. Consider a liter of surficial mud with 5% (dry weight) of early diagenetic pyrite, 80% porosity (filled with water), and 1 mM dissolved pore water sulfide (H_2S). Pore-water sulfide concentrations of ~ 1 mM are typical for pore waters of surficial Santa Barbara Basin muds that accumulate under suboxic conditions (Reimers et al. 1996). In that scenario, early diagenetic pyrite contributes 99.5% of the sulfide pool available for oxidation. If partial oxidation were to destroy a mere 10% of that pyrite, it would contribute the bulk (95%) of the sulfide for acid production.
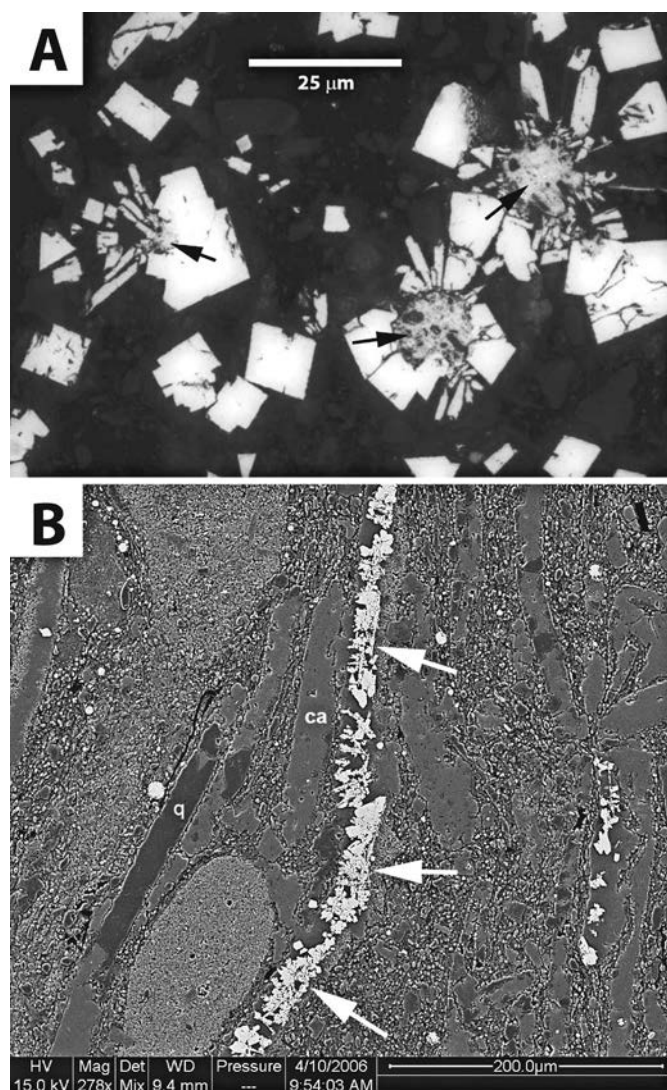
FIG. 11.—**A)** Marcasite in carbonaceous shale of the Pennsylvanian Cisco Formation of Texas (Sur 2009). The reflected-light photomicrograph shows central bodies (black arrows) of diagenetic pyrite (possibly cemented pyrite framboids) that are overgrown with radial-bladed marcasite (identified by optical properties and EBSD). **B)** SEM photomicrograph (backscatter image) of marcasite-bearing sample of Barnett Shale with calcareous ("ca") brachiopod shells. This image shows in the center a brachiopod shell (white arrows) that is partially replaced by marcasite (bright dendritic grains; large equant bright grains are pyrite), and partial silica ("q") replacement of adjacent brachiopod shell.

Typical pyrite framboids that form in natural and experimental sediments are spherical and composed of densely packed crystallites (Wilkin 2003; see Fig. 7B for example). Remnant spherical shapes (Figs. 1A, 2A, 7D) are suggestive of degradation and deformation of original pyrite framboids that have suffered partial dissolution. Regular framboids, because they consist of tightly packed pyrite microcrysts, are not appreciably affected by compaction of their host shale (Fig. 3B), and to allow for deformation, the removal of a portion of the original crystallites is required. Remnant spherical shapes have the shape and size of pyrite framboids, but a portion of the constituent crystallites is missing. Inclusion into early diagenetic quartz cement (Fig. 7D) can protect these features from compaction, and their shape and size is consistent with a pyrite framboid origin followed by framboid microcryst dissolution in the course of marcasite formation. Black shales also typically contain
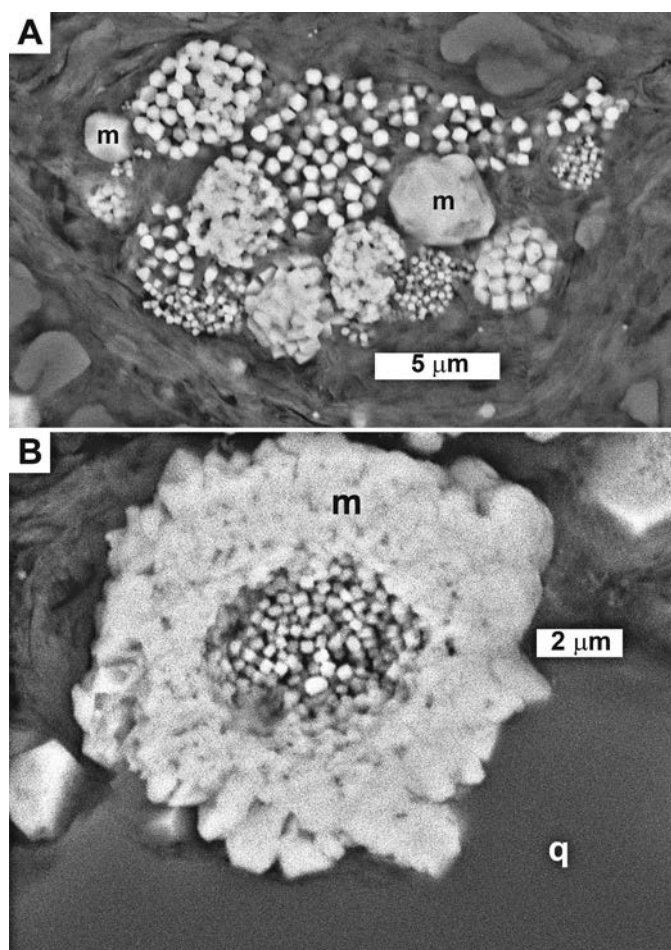
FIG. 12.—SEM backscatter images of marcasite in carbonaceous shales of the Powers Steps Formation of Newfoundland (Arenig, Ordovician). **A)** Polyframboid cluster with remnant spherical shapes (interpreted as degraded pyrite framboids), pyrite patches, and some marcasite ("m"). Note differential compaction around iron sulfide body. **B)** Pyrite framboid with coarser crystalline overgrowth that was identified as marcasite ("m") with EBSD. Note that the marcasite is enclosed in diagenetic quartz (medium gray, "q") in the lower half of the image.

irregular patches of pyrite microcrysts in addition to framboids (e.g., Wignall and Newton 1998). Whereas some of these may be degraded framboids, others are quite likely primary. Pyrite microcrysts of both framboids and patches are likely to react and provide dissolved iron and acidity (Eq. 1) when oxygen diffuses into the sediment.

In millimeter- to centimeter-size pyrite grains of marine lags, corrosion features are readily visible (Schieber 2007; Schieber and Riciputi 2005). In the case of sub-micrometer pyrite crystallites, however, visual evidence of corrosion is considerably more difficult to obtain. At a surface/volume ratio that is three to four orders of magnitude larger than that of dissolving pyrite grains in lags (Schieber 2007), it is much more likely that microcrysts will dissolve completely, rather than partially. As a consequence, rather than producing corrosion features on crystallite surfaces, pyrite oxidation will more likely result in dissolution gaps and a reduced crystallite density within pyrite framboids. The observations of remnant spherical shapes (Figs. 1A, 2A, 7D) are consistent with this scenario. Corroded framboid surfaces (Fig. 7A) and corrosion features in micro-concretions (Fig. 9C) provide further support for the notion of pyrite dissolution associated with marcasite formation.

The convergence of chemical considerations, observations from modern environments, and textural observations from the rock record

strongly suggests that marcasite can form in marine mud via partial oxidation of carbonaceous, previously anoxic sediments. In this conceptual model, oxidation of sedimentary pyrite (via Eq. 1) decreases the pore-water pH and increases concentrations of dissolved iron. Hydrogen sulfide generated in reducing micro-environments, such as organic cysts, radiolarian tests, and in underlying sediments, can combine with the dissolved iron to precipitate marcasite. Evidence for dissolution of phosphatic and calcitic fossil debris (Figs. 5, 7C, 11B) is consistent with the interpretation of marcasite formation at reduced pore-water pH, and is corroborated by association and intergrowth of marcasite with authigenic quartz (Figs. 3B, 7C, 8B, 11B) and kaolinite (Fig. 2B). Low pH favors precipitation of quartz and kaolinite from solution and drives replacement of calcite (Blatt 1992; Faure 1998).

In this scenario, it is conceivable that some of the ferrous iron (Fe^{2+}) (e.g., Eq. 1) is oxidized to ferric iron (Fe^{3+}) near the sediment–water interface. Because Fe^{3+} is a strong oxidizing agent (Singer and Stumm 1970), the question of how iron cycling would affect the chemical conditions for marcasite precipitation is of interest. Because it is unlikely that reactable ferric iron is present in an organic-rich mud prior to an oxidation event, a precondition for Fe^{3+} presence is initial oxidation of pyrite according to Eq. 1, producing two H^+ for each FeS_2 destroyed. The oxidation of one Fe^{2+} would consume one H^+ according to Eq. 2:

$$4Fe^{2+} + O_2 + 4H^+ \quad 4Fe^{3+} + 2H_2O \qquad (2)$$
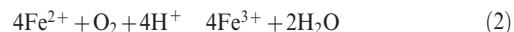
At first glance, this reaction would seem to suggest that the initially produced acidity is cut in half. This "loss," however, is counterbalanced via Eq. 3 (McKibben and Barnes 1986), wherein Fe^{3+} oxidizes pyrite:

$$FeS_2 + 14Fe^{3+} + H_2O \quad 15Fe^{2+} + 2SO_4^2 + 16H^+ \qquad (3)$$
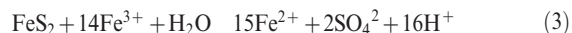
Adding and balancing these equations shows that for each FeS_2 that is destroyed there is a net production of $2H^+$. Thus, any Fe^{3+} to Fe^{2+} iron cycling that may occur does not affect the net pH effect due to the initial oxidation reaction (Eq. 1). Furthermore, because the reaction rate for Eq. 3 is three orders of magnitude lower than that of Eq. 1 (McKibben and Barnes 1986), the pH conditions in the pore waters are mostly controlled by Eq. 1.

In this context, it is worth noting that oxidation of marcasite produces acidity just as effectively as the oxidation of pyrite discussed above. Thus, it is perfectly conceivable that first-generation marcasite in a black shale can itself be oxidized by subsequent oxidation events and give rise, depending on pH, to successive generations of marcasite or pyrite. Multiple oxidation events of that kind have been documented from sandy marine sediments (Schieber and Riciputi 2005; Schieber 2007) and might be revealed in shales through high-resolution electron microscopy and EBSD mapping.

Although marcasite in black shales was the focus of this study, low-TOC gray shale beds in the sample collections were also examined. Gray shale beds contain early diagenetic pyrite as well and presumably were deposited under more oxygenated bottom waters. Thus, one might expect that during reworking and bioturbation, gray shales should also experience intermittent and/or localized reoxidation of sedimentary iron sulfides. One should therefore expect to find marcasite in gray shale beds as well. Reflected light microscopy of gray shale beds from Devonian black shale intervals, the Winnipeg Formation, and the Power Steps Formation (Table 1) bears out this assumption.

CONCLUDING THOUGHTS

Mineralization of organic matter in marine sediments is linked to oceanic cycling of iron and sulfur, the buildup of oxygen in the earth's

atmosphere, and global climate (Berner 2001). Episodes of enhanced organic-carbon burial, marked by globally extensive deposits of black shales and at times by mass extinctions (Hallam and Wignall 1997), are thus of particular interest, and beg the question whether marcasite formation via postdepositional oxidation of carbonaceous muds could have a potential impact on carbon burial and global climate.

In fully oxygenated seawater, sedimentary pyrite initially oxidizes quite rapidly, with sub-micrometer grains reacting completely within weeks to months, whereas larger grains (1–10 micrometer) react more slowly, requiring from months to years for complete destruction (Morse 1991). The initial high reaction rates (Morse 1991) probably mark the time interval that could be considered most conducive to marcasite formation because dissolved-iron concentrations and acidity would be at their peak. Judging from Morse's (1991) experiments, lower oxygen concentrations should expand this initial time interval, possibly to as much as several years. In contrast to the marcasite reoxidation scenario, the better-known cases of downward oxidation, commonly described as burn-down, involve complete destruction of iron sulfides and organic matter, and require time spans on the order of thousands to ten thousands of years (e.g., Higgs et. al 1994; Jung et al. 1997). Because burn-down also involves the loss of dark sediment coloration, it is comparatively easy to recognize in the rock record. Reoxidation events that produce marcasite, on the other hand, are easily missed because oxidation mainly affects the sulfides, leaves the organic matter largely intact, and has little effect on the overall color of the sediment.

In the examples presented here, partial preservation of original pyrite (Figs. 2A, 8A) and an abundance of preserved organic matter implies that, in contrast to what would be expected during burn-down, marcasite formation represents small-scale oxidation events of much shorter duration. Because these oxidation events did not even destroy all of the original sedimentary pyrite, it is unlikely that the organic-matter content of the sediment was lowered much. Thus, the potential impact of marcasite-producing oxidation events on carbon burial rates and climate must be considered negligible. However, because these events inform about the long-term oxygenation state of the water column, they are nonetheless important. A case-by-case assessment is required to determine whether early diagenetic marcasite in a black shale implies a lack of bottom water anoxia, an influx of oxygenated waters together with intermittent sediment pulses (Föllmi and Grimm 1990), or intermittent thermohaline circulation of dense oxygenated water masses.

The occurrence of marcasite in multiple black shale intervals (Table 1) has implications for understanding Earth history and raises other questions. For example, if early diagenetic marcasite indicates intermittent reoxidation of accumulating carbonaceous muds, would its absence imply a continuously anoxic water column? Or, because oxygen is brought in via water circulation, would a systematic examination of the rock record suggest that even during so called oceanic anoxia the oceans were at least intermittently oxygenated, or at least more than previously assumed? If marcasite is pervasive in OAE shales, why is bioturbation not equally pervasive? Because marcasite precipitates much faster than pyrite once conditions are right (Schoonen and Barnes 1991), does this imply that the marcasite producing reoxidation events were of too short of a duration to allow deep benthos to be colonized? Alternatively, could low-pH pore waters be detrimental to benthos? Also, for marcasite formation in OAE shales, could its presence imply injection of oxygenated waters by current events, whilst a largely anoxic water column would still have acted as a barrier for benthic organisms? Understanding the significance and role of early diagenetic marcasite formation in Precambrian black shales (Fig. 9) may also provide a new avenue of inquiry for research into the oxygenation state of Precambrian oceans (Canfield 2005).

Uncritical application of any proxy invites erroneous interpretation of the rock record, and the "marcasite proxy" is no exception. It can be taken to indicate early diagenetic reoxidation only if marcasite formation

occurred in uncompacted, water-rich sediments (Figs. 2C, 4, 9A). Many paleoceanographic proxies, including redox proxies (Jones and Manning 1994; Sageman et al. 2003) are based on trace metals contained in carbonaceous muds. Marcasite formation, accompanied by redox shifts, low pH, and sulfide dissolution, has clear potential to substantially alter trace-metal-based paleoceanographic proxies.

REFERENCES

ALVI, K., AND WINTERHALTER, B., 2001, Authigenic mineralisation in the temporally anoxic Gotland Deep, the Baltic Sea: Baltica, v. 14, p. 74–83.

BEN-YAAKOV, S., 1973, pH buffering of pore waters of recent anoxic marine sediments: Limnology and Oceanography, v. 18, p. 86–94.

BENNING, L.G., WILKIN, R.T., AND BARNES, H.L., 2000, Reaction pathways in the Fe-S system below 100°C: Chemical Geology, v. 167, p. 25–51.

BERNER, R.A., 1984, Sedimentary pyrite formation: an update: Geochimica et Cosmochimica Acta, v. 48, p. 605–615.

BERNER, R.A., 2001, Modeling atmospheric O_2 over Phanerozoic time: Geochimica et Cosmochimica Acta, v. 65, p. 685–694.

BLATT, H., 1992. Sedimentary Petrology [2nd edition]: New York, W.H. Freeman & Co., 514 p.

BUSH, R.T., MCGRATH, R., AND SULLIVAN, L.A., 2004, Occurrence of marcasite in an organic-rich Holocene estuarine mud: Australian Journal of Soil Research, v. 42, p. 617–621.

CANFIELD, D.E., 2005, The early history of atmospheric oxygen: Annual Reviews of Earth and Planetary Sciences, v. 33, p. 1–36.

CECCA, F., MARINI, A., PALLINI, G., BAUDIN, F., AND BEGOUEN, V., 1994, A guide-level of the uppermost Hauterivian (Lower Cretaceous) in the pelagic succession of Umbria–Marche Apennines (Central Italy): the Faraoni Level: Rivista Italiana di Paleontologia e Stratigrafia, v. 99, p. 551–568.

CONANT, L.C., AND SWANSON, V.E., 1961, Chattanooga shale and related rocks of central Tennessee and nearby areas: U.S. Geological Survey, Professional Paper 357, 91 p.

COLEMAN, M.L., 1985, Geochemistry of diagenetic non-silicate minerals: kinetic considerations: Royal Society of London, Philosphical Transactions, v. A 315, p. 39–56.

DUMITRESCU, M., 2006. High-resolution biogeochemical study of organic-rich sediments from the early Aptian oceanic anoxic event at Shatsky Rise, ODP Leg 198 [Ph.D. Dissertation]: Indiana University, Bloomington, 212 p.

DUMITRESCU, M., AND BRASSELL, S.C., 2005, Biogeochemical assessment of sources of organic matter and paleoproductivity during the early Aptian oceanic anoxic event at Shatsky Rise, ODP Leg 198: Organic Geochemistry, v. 36, p. 1002–1022.

DUMITRESCU, M., AND BRASSELL, S.C., 2006, Compositional and isotopic characteristics of organic matter for the early Aptian Oceanic Anoxic Event at Shatsky Rise, ODP Leg 198: Palaeogeograpy, Palaeoclimatology, Palaeoecology, v. 235, p. 168–191.

DUMITRESCU, M., BRASSELL, S.C., SCHOUTEN, S., HOPMANS, E.C., AND SINNINGHE DAMSTE, J.S., 2006, Instability in tropical Pacific sea-surface temperatures during the early Aptian: Geology, v. 34, p. 833–836.

FAURE, G., 1998. Principles and Applications of Geochemistry: A Comprehensive Textbook for Geology Students: Upper Saddle River, N.J., Prentice Hall, 600 p.

GOLDHABER, M.B., 2003, Sulfur-rich sediments, *in* Mackenzie, F.T., ed., Treatise on Geochemistry, v. 7: Sediments, Diagenesis, and Sedimentary Rocks: Amsterdam, Elsevier, p. 257–288.

FÖLLMI, K.B., AND GRIMM, K.A., 1990, Doomed pioneers: Gravity-flow deposition and bioturbation in marine oxygen-deficient environments: Geology, v. 18, p. 1069–1072.

FÜCHTBAUER, H., 1988, Sedimente und Sedimentgesteine: Stuttgart, Schweizerbart, 1141 p.

GOLDRING, R., 1995, Organisms and the substrate: response and effect, *in* Bosence, D.W.J., and Allison, P.A., eds., Marine Paleoenvironmental Analysis from Fossils, Geological Society of London, Special Publication 83, p. 151–180.

HALLAM, A., AND WIGNALL, P.B., 1997. Mass Extinctions and Their Aftermath: Oxford, U.K., Oxford University Press, 328 p.

HAYES, J.B., 1991, Porosity evolution of sandstones related to vitrinite reflectance: Organic Geochemistry, v. 17, p. 117–129.

HIGGS, N.C., THOMSON, J., WILSON, T.R.S., AND CROUDACE, I.W., 1994, Modification and complete removal of eastern Mediterranean sapropels by postdepositional oxidation: Geology, v. 22, p. 423–426.

JONES, B., AND MANNING, D.A.C., 1994, Comparison of geochemical indices used for the interpretation of palaeoredox conditions in ancient mudstones: Chemical Geology, v. 111, p. 111–129.

JUNG, M., ILMBERGER, J., MANGINI, A., AND EMEIS, K.-C., 1997, Why some Mediterranean sapropels survived burn-down (and others did not): Marine Geology, v. 141, p. 51–60.

KRUMBEIN, W.C., AND GARRELS, R.M., 1952, Origin and classification of chemical sediment in terms of pH and oxidation-reduction potentials: Journal of Geology, v. 60, p. 1–33.

LOBZA, V., AND SCHIEBER, J., 1999, Biogenic sedimentary structures produced by worms in soupy, soft muds: observations from the Chattanooga Shale (Upper Devonian) and experiments: Journal of Sedimentary Research, v. 69, p. 1041–1049.

LUTHER, G.W., AND CHURCH, T.M., 1988, Seasonal cycling of sulfur and iron in porewaters of a Delaware salt marsh: Marine Chemistry, v. 23, p. 295–309.

MARSAGLIA, K.M., 2005, Sedimentology, petrology, and volcanology of the lower Aptian Oceanic Anoxic Event (OAE1a), Shatsky Rise, north-central Pacific Ocean, in Bralower, T.J., Premoli Silva, I., and Malone, M.J., eds., Proceedings of the Ocean Drilling Project, Scientific Results, v. 198, p. 1–31, [Online].

MACGOWAN, D.B., AND SURDAM, R.C., 1990, Carboxylic acid anions in formation waters, San Joaquin Basin and Louisiana Gulf Coast, U.S.A.—implications for clastic diagenesis: Applied Geochemistry, v. 5, p. 687–701.

MILLIKEN, K., CHOH, S.-J., PAPAZIS, P., AND SCHIEBER, J., 2007, "Cherty" stringers in the Barnett Shale are agglutinated foraminifera: Sedimentary Geology, v. 198, p. 221–232.

MORSE, J.W., 1991, Oxidation kinetics of sedimentary pyrite in seawater: Geochimica et Cosmochimica Acta, v. 55, p. 3665–3667.

MUROWCHICK, J.B., AND BARNES, H.L., 1987, Effects of temperature and degree of supersaturation on pyrite morphology: American Mineralogist, v. 72, p. 1241–1250.

RAMDOHR, P., 1980. The ore minerals and their intergrowths, second Edition, 2 vols.: Oxford, U.K., Pergamon Press, 1205 p.

RANGER, M.J., PICKERILL, R.K., AND FILLION, D., 1984, Lithostratigraphy of the Cambrian? –Lower Ordovician Bell Island and Wabana groups of Bell, Little Bell, and Kelly Islands, Conception Bay, eastern Newfoundland: Canadian Journal of Earth Sciences, v. 21, p. 1245–1261.

RAY, J.S., 2006, Age of the Vindhyan Supergroup: a review of recent findings: Journal of Earth System Science, v. 115, p. 149–160.

REAVES, C.M., 1986, Organic matter metabolizability and calcium carbonate dissolution in nearshore marine muds: Journal of Sedimentary Petrology, v. 56, p. 486–494.

REIMERS, C.E., RUTTENBERG, K.C., CANFIELD, D.E., CHRISTIANSEN, M.B., AND MARTIN, J.B., 1996, Porewater pH and authigenic phases formed in the uppermost sediments of the Santa Barbara Basin: Geochimica et Cosmochimica Acta, v. 60, p. 4037–4057.

RICKARD, D., SCHOONEN, M.A.A., AND LUTHER, G.W., 1995, Chemistry of iron sulfides in sedimentary environments, in Vairavamurtry, M.A., and Schoonen, M.A.A., eds., Geochemical Transformations of Sedimentary Sulfur, American Chemical Society, Symposium Series 612, Washington, p. 165–193.

SAGEMAN, B.B., MURPHY, A.E., WERNE, J.P., VER STRAETEN, C.A., HOLLANDER, D.J., AND LYONS, T.W., 2003, A tale of shales: the relative roles of production, decomposition, and dilution in the accumulation of organic-rich strata, Middle–Upper Devonian, Appalachian basin: Chemical Geology, v. 195, p. 229–273.

SCHIEBER, J., 2007, Oxidation of detrital pyrite as a cause for marcasite formation in marine lag deposits from the Devonian of the eastern US: Deep-Sea Research II, v. 54, p. 1312–1326.

SCHIEBER, J., 2009, Discovery of agglutinated benthic foraminifera in Devonian black shales and their relevance for the redox state of ancient seas: Palaeogeography, Palaeoclimatology, Palaeoecology, v. 271, p. 292–300.

SCHIEBER, J., AND BAIRD, G., 2001, On the origin and significance of pyrite spheres in Devonian black shales of North America: Journal of Sedimentary Research, v. 71, p. 155–166.

SCHIEBER, J., and LAZAR, R.O., eds., Devonian Black Shales of the Eastern U.S.: New Insights into Sedimentology and Stratigraphy from the Subsurface and Outcrops in the Illinois and Appalachian Basins: Great Lakes Section, SEPM Annual Field Conference, Field Guide: Indiana Geological Survey, Open File Study 04-05, 90 p.

SCHIEBER, J., AND RICIPUTI, L., 2005, Pyrite-marcasite coated grains in the Ordovician Winnipeg Formation, Canada: an intertwined record of surface conditions, stratigraphic condensation, geochemical "reworking," and microbial activity: Journal of Sedimentary Research, v. 75, p. 905–918.

SCHIEBER, J., SUR, S., AND BANERJEE, S., 2007, Benthic microbial mats in black shale units from the Vindhyan Supergroup, Middle Proterozoic of India: the challenges of recognizing the genuine article, in Schieber, J., et al. (2007). Atlas of Microbial Mat Features Preserved within the Clastic Rock Record: Amsterdam, Elsevier, p. 189–197.

SIESSER, W.G., 1978, Petrography and geochemistry of pyrite and marcasite in DSDP Leg 40 sediments: Initial Reports of the Deep Sea Drilling Project, Supplement to Volumes 38, 39, 40, and 41, p. 767–775.

SINGER, P.C., AND STUMM, W., 1970, Acid mine drainage —the rate determining step: Science, v. 167, p. 1121–1123.

SCHOONEN, M.A.A., AND BARNES, H.L., 1991, Reactions forming pyrite and marcasite from solution. I. Nucleation of FeS_2 below 100° C: Geochimica et Cosmochimica Acta, v. 55, p. 1495–1504.

SUR, S., 2009. An integrated sedimentological and geochemical study to test the possible links between late Paleozoic climate change, atmospheric dust influx and primary productivity in the Horseshoe Atoll, West Texas [Unpublished Ph.D. dissertation]: University of Oklahoma, 137 p.

SURDAM, R.C., CROSSEY, L.C., HAGEN, S.V., AND HEASLER, H.P., 1989, Organic–inorganic and sandstone diagenesis: American Association of Petroleum Geologists, Bulletin, v. 73, p. 1–23.

SURDAM, R.C., MACGOWAN, D.B., AND DUNN, T.L., 1991, Predictive models for sandstone diagenesis: Organic Geochemistry, v. 17, p. 243–253.

WIGNALL, P.B., AND NEWTON, R., 1998, Pyrite framboid diameter as a measure of oxygen-deficiency in ancient mudrocks: American Journal of Science, v. 298, p. 537–552.

WILKIN, R.T., 2003, Sulfide minerals in sediments, in Middleton, G.V., ed., Encyclopedia of Sediments and Sedimentary Rocks: New York, Kluwer Academic Publishers, p. 701–703.

WILSON, B.P., 2005, Classification issues for the Hydrosol and Organosol Soil Orders to better encompass surface acidity and deep sulfidic horizons in acid sulfate soils: Australian Journal of Soil Research, v. 43, p. 629–638.